ACS APPLIED MATERIALS & INTERFACES

Research Article

www.acsami.org

Energy-Cascade Organic Photovoltaic Devices Incorporating a Host–Guest Architecture

S. Matthew Menke and Russell J. Holmes*

Department of Chemical Engineering and Materials Science, University of Minnesota, 421 Washington Ave SE, 151 Amundson Hall, Minneapolis, Minnesota 55455, United States

Supporting Information

ABSTRACT: In planar heterojunction organic photovoltaic devices (OPVs), broad spectral coverage can be realized by incorporating multiple molecular absorbers in an energy-cascade architecture. Here, this approach is combined with a host–guest donor layer architecture previously shown to optimize exciton transport for the fluorescent organic semiconductor boron subphthalocyanine chloride (SubPc) when diluted in an optically transparent host. In order to maximize the absorption efficiency, energy-cascade OPVs that utilize both photoactive host and guest donor materials are examined using the pairing of SubPc and boron subnaphthalocyanine chloride (SubNc), respectively. In a planar heterojunction architecture, excitons generated on the SubPc host rapidly energy transfer to the SubNc guest, where they may migrate toward the dissociating, donor–acceptor interface. Overall, the incorporation of a photoactive host leads to a 13% enhancement in the short-circuit current density and a 20% enhancement in the power conversion efficiency relative to an optimized host–guest OPV combining SubNc with a nonabsorbing host. This work underscores the potential for further design refinements in planar heterojunction OPVs and demonstrates progress toward the effective separation of functionality between constituent OPV materials.

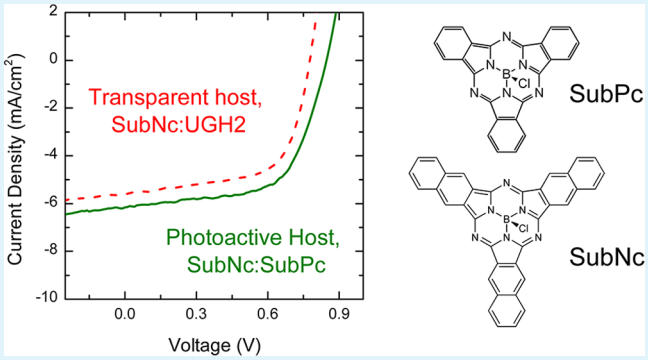

KEYWORDS: *exciton, diffusion, OPV, SubPc, SubNc, cascade, energy transfer*

1. INTRODUCTION

Recent advances in organic photovoltaic device (OPV) power conversion efficiency (η_P) have often mirrored improvements in understanding the role of nanoscale morphology in photoconversion.[1−3] In large part, OPVs have realized significant gains in η_P by optimizing the bulk heterojunction architecture, where the electron-donating and -accepting materials are blended to ensure efficient exciton harvesting.[4−6]

Careful attention must be paid to the optimization of film morphology in these architectures in order to ensure that photogenerated charge carriers are collected efficiently, thereby minimizing losses due to nongeminate recombination.[7−10] In planar heterojunction OPVs, the typically short exciton diffusion length (L_D) establishes a trade-off between optical absorption and efficient exciton harvesting, limiting η_P.[11] In contrast to the bulk heterojunction, however, the planar heterojunction OPV architecture inherently resists nongeminate recombination since there is a smaller spatial cross-section for electron and hole overlap.[12] Relaxed constraints on efficient carrier collection are advantageous, provided routes for enhanced L_D and exciton harvesting can be devised. Recently, OPVs with enhanced L_D and exciton harvesting efficiencies have been demonstrated through techniques such as dilution,[13] chemical modification,[14] microcrystallization,[15] cascade energy transfer,[16−21] and others.[22−24]

In the case of dilution, variation of the intermolecular spacing optimizes the rate of intermolecular Förster energy transfer through photophysical properties such as the photoluminescence efficiency. This enhancement in energy transfer is directly correlated to enhancements in L_D. Previous work experimentally demonstrates this technique by diluting the electron-donating species, boron subphthalocyanine chloride (SubPc), into a wide energy-gap host material, *p*-bis(triphenylsilyl)-benzene (UGH2).[13] The L_D increases from L_D = 10.7 nm in a neat film of SubPc to L_D = 15.4 nm for a film containing 25 wt % SubPc diluted in UGH2. Devices constructed using a dilute layer of SubPc in UGH2 show a 30% enhancement in η_P. Increases in both the short-circuit current density (J_{SC}) and η_P were observed despite a concomitant ∼30% decrease in donor absorption. The decrease in absorption efficiency results from the wide-energy gap of UGH2.[25] This suggests that there is the potential for increased photocurrent if the host material was also photoactive.

Organic photovoltaic devices incorporating more than two absorbing species have been widely explored in a variety of incarnations. Of note are cascade OPVs, where two exciton

Received: November 26, 2014
Accepted: January 12, 2015
Published: January 22, 2015

DOI: 10.1021/am508332n
ACS Appl. Mater. Interfaces 2015, 7, 2912−2918

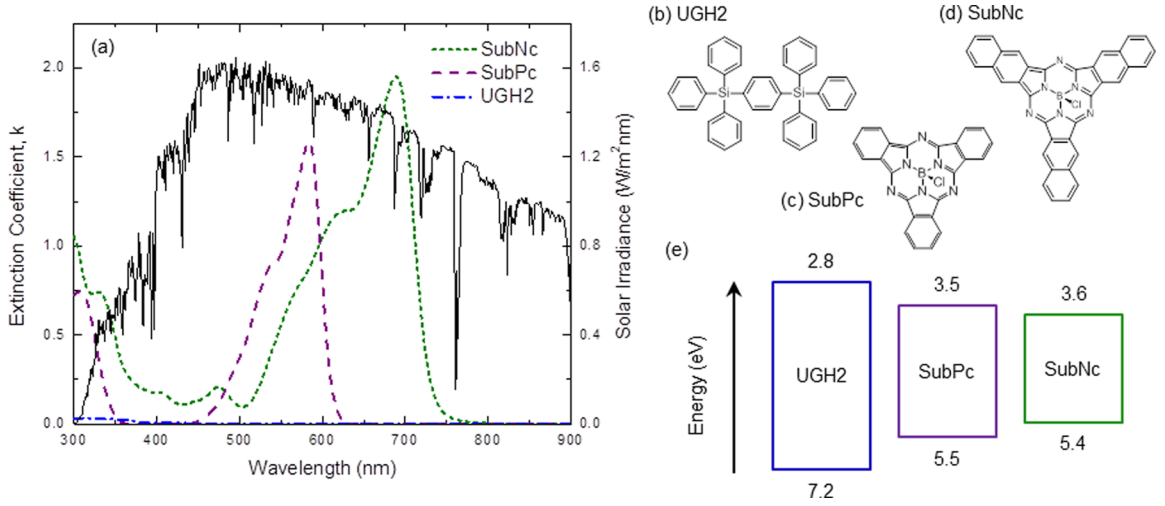

Figure 1. (a) Thin film spectral extinction coefficient for SubPc, SubNc, and UGH2 as compared to the AM1.5G solar spectrum (solid line). (b–d) Molecular structures and (e) molecular orbital energy levels for SubPc, SubNc, and UGH2.

dissociating interfaces are formed between three molecular species with staggered molecular orbital energy levels.[26−29] In contrast, energy-cascade OPVs contain a single dissociating interface and incorporate composite donor or acceptor layers (i.e., contain more than a single molecular species).[18,21,30] The composite layers can be implemented as multilayer stacks as well as mixtures thereof. In this work, the dilute donor concept is applied to demonstrate energy-cascade OPVs that utilize a host−guest donor layer.

Boron subnaphthalocyanine chloride (SubNc) was selected as a guest material to integrate with a photoactive host of SubPc.[31] SubPc and SubNc have been previously used as complementary absorbers in tandem OPVs.[32] Figure 1 shows the extinction coefficient and molecular orbital energy levels for SubNc,[17] SubPc,[17] and UGH2.[25] Owing to its wide energy-gap (E_g = 4.4 eV), UGH2 does not strongly absorb in the solar spectrum (Figure 1a). Excitons generated on SubPc (E_g = 2 eV) neither energy transfer to UGH2 nor dissociate in the presence of UGH2, creating a single pathway for exciton transport. SubNc also strongly absorbs in the visible spectrum with a reduced energy-gap (E_g = 1.8 eV) relative to SubPc. When SubNc is diluted in SubPc, two donor exciton harvesting pathways exist in parallel. Similar to the case of dilute SubPc, excitons generated on SubNc diffuse along a pathway composed of SubNc molecules toward the donor−acceptor interface. The difference in energy-gap between SubNc and SubPc is much larger than the ambient thermal energy (~25 meV), ensuring that excitons generated on SubNc do not energy transfer to SubPc. In this way, SubPc acts analogously to UGH2. A second pathway is also present for excitons that originate on SubPc. Efficient Förster energy transfer from SubPc to SubNc occurs rapidly,[16] and excitons may follow the same route to the interface as those originally generated on SubNc. Overall, all photogenerated excitons are quickly confined to molecules of SubNc followed by short-range exciton energy transfer toward the donor−acceptor interface where excitons are dissociated. Here, the host−guest donor layer is distinct from composite donor layers formed from multilayer stacks as the photogenerated charges remain solely on the guest species (SubNc) during transport toward the anode.

2. RESULTS AND DISCUSSION

2.1. Exciton Diffusion in SubNc. The exciton transport properties of dilute SubNc films were separately investigated in order to determine if a dilute donor enhancement in L_D is also observed for SubNc. Additionally, this characterization provides guidance for selecting appropriate dilute film concentrations to be used during device fabrication. The diffusive behavior (L_D) of excitons in films of SubNc as a function of concentration is measured via spectrally resolved photoluminescence quenching[33,34] (SRPLQ) as a function of dilution in UGH2. For example, Figure 2a shows the measured photoluminescence emission and excitation spectra for a 75 nm-thick film of 25 wt % SubNc in UGH2. Experimental photoluminescence quenching ratios (PL ratios) are constructed by measuring the photoluminescence excitation spectrum of a SubNc:UGH2 film deposited on a 15 nm-thick quenching layer of 1,4,5,8,9,11-hexaazatriphenylene hexacarbonitrile[35] (HATCN) and dividing it by the excitation spectrum of an identical film of SubNc:UGH2 deposited on a glass substrate. Optical transfer matrix simulations combined with analytical solutions to the exciton diffusion equation allow for the simulation of predicted PL ratios which are sensitive to the L_D of the film.[36] Iterative fitting of the measured and predicted PL ratios allows for the determination of L_D. SRPLQ measurements were performed over a range of film thicknesses between 75 and 125 nm. The experimental PL ratios and respective fits for three thicknesses of 25 wt % SubNc in UGH2 films are shown in Figure 2b. The resulting fit values for L_D are L_D = 25.8, 26.5, and 34.0 nm for films that are 75, 100, and 125 nm thick, respectively. SRPLQ measurements of L_D were also performed for films of 5, 10, and 50 wt % SubNc in UGH2. The measured PL ratios and respective fits for these additional concentrations can be found in the Supporting Information. Good fits to the measured PL ratios were obtained in spectral regions corresponding to strong SubNc absorption (~550−700 nm). Deviations observed in the shorter wavelength spectral regions (~400−550 nm) are likely due to the low signal intensity characteristic of spectral bands with low extinction coefficients. These deviations are then propagated into the overall fit value for L_D and result in a broader range of L_D values for a given concentration than typically obtained using thickness-dependent photoluminescence quenching-based techniques.[11] Figure 2c summarizes the

DOI: 10.1021/am508332n
ACS Appl. Mater. Interfaces 2015, 7, 2912−2918

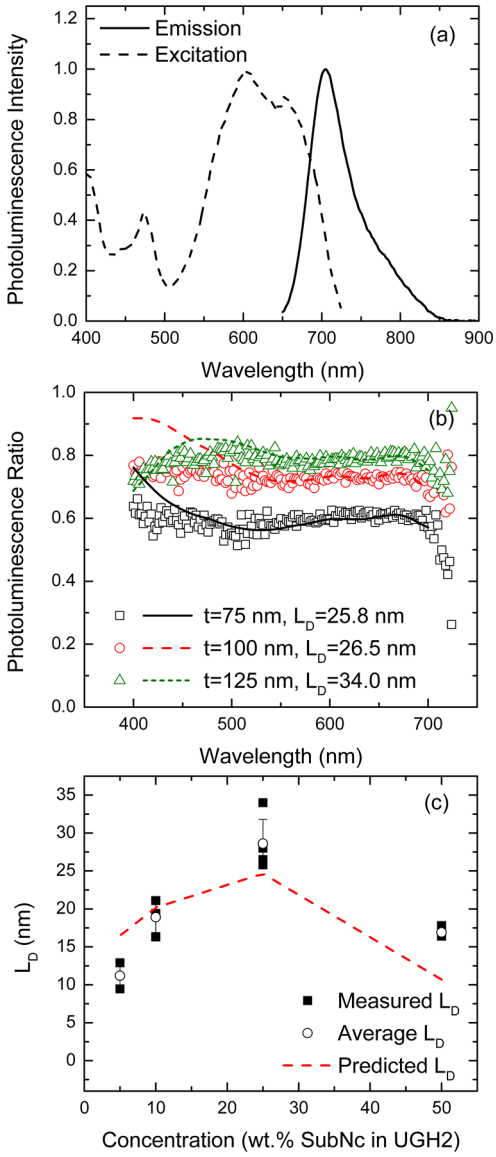

Figure 2. (a) Normalized excitation and emission spectra for a film of 25 wt % SubNc dispersed in UGH2. (b) Spectrally resolved photoluminescence ratios for three films of 25 wt % SubNc dispersed in UGH2 of varying thickness (t) along with the corresponding fit and fit value for the L_D. (c) Summary of L_D fit values for films of SubNc dispersed in UGH2 as a function of concentration. Also shown is the average L_D at each concentration where the error bars represent the standard deviation in L_D over the range of thicknesses measured.

measured values of L_D versus film concentration where each data point reflects a different film thickness at a given concentration. Also shown is the average L_D for each concentration where the error bars reflect the standard deviation. SRPLQ measurements of neat SubNc were not possible due to the low photoluminescence efficiency (η_{PL}) of films of pure SubNc ($\eta_{PL} \leq 0.25\%$). However, preliminary device-based measurements combined with modeling of the external quantum efficiency (η_{EQE}) suggest the L_D for pure SubNc is $L_D \sim 11$ nm. This result, however, is susceptible to error where, for example, a nonunity charge collection efficiency (η_{CC}) will lead to an underestimate of L_D. Interestingly, the L_D of SubNc exhibits a dependence on concentration (Figure 2c). As in the case of SubPc, diffusion is not optimized in neat films of SubNc, and a near tripling of L_D is found in 25 wt % SubNc in UGH2 films compared to the approximate L_D in pure films.

For fluorescent organic semiconductors, the Förster theory of energy transfer has been successfully applied to a variety of systems.[13,14,37,38] Here, we apply Förster theory to describe exciton diffusion in SubNc as a function of dilution in UGH2. By assuming that exciton diffusion is dominated by nearest neighbor Förster energy transfer, predictions for the L_D of SubNc as a function of concentration can be made. The L_D as predicted from this simple interpretation of Förster energy transfer is written as[33,37,39]

$$L_D = \frac{R_0^3}{d^2} = \frac{1}{d^2}\sqrt{\frac{9\eta_{PL}\kappa^2}{128\pi^5 n^4}\int \lambda^4 F_D(\lambda)\sigma_A(\lambda)d\lambda} \quad (1)$$

where R_0 is the self-Förster radius, d is the average intermolecular separation, κ is the dipole orientation factor, n is the index of refraction at maximum absorption-emission overlap, λ is the wavelength, F_D is the area normalized fluorescence, and σ_A is the absorption cross section. Here, randomly oriented rigid dipoles are used to approximate the amorphous nature of the films with $\kappa = 0.845(2/3)^{1/2}$.[40] The value of n is determined from separate measurements of the optical constants via spectroscopic ellipsometry. The absorption cross-section is defined as the absorption coefficient divided by the molecular density of the film (ρ). Here, d is taken to be the Wigner-Seitz radius as tabulated from $d = (3/(4\pi\rho))^{1/3}$. The tabulated predictions for the SubNc L_D when dispersed in UGH2 are shown in Figure 2c, showing good agreement with the experimentally measured L_D values.

2.2. Dilute SubNc Devices with a Nonabsorbing Host.

In order to confirm the robustness of photoconversion in SubNc to dilution, host−guest OPVs were fabricated incorporating UGH2 as the host material (Figure 3). A 10 nm-thick layer of MoO_x acts as the anode buffer layer[41] and a 10 nm-thick layer of bathocuproine (BCP) acts as the cathode buffer layer.[42] A 150 nm-thick layer of indium tin oxide (ITO) and a 100 nm-thick layer of Al serve as the anode and cathode, respectively. A multilayer donor scheme consisting of a 10 nm-thick dilute layer followed by a 3 nm-thick neat layer of SubNc constitutes the effective donor layer. A thin, neat layer of SubNc is inserted at the donor−acceptor interface. This partially offsets the reduction in absorption efficiency upon dilution and is placed in a location where exciton harvesting is already efficient. Figure 3 shows the J_{SC}, open-circuit voltage (V_{OC}), fill factor, and η_P as a function of the dilute layer concentration collected at an intensity of 100 mW/cm^2 under AM1.5G solar simulated illumination. The open symbols correspond to a neat film of SubNc and represent a control device with a single donor layer consisting of a 13 nm-thick layer of SubNc. A summary of the performance for undiluted SubNc devices as a function of donor layer thickness can be found in the Supporting Information.

Interestingly, the J_{SC} is relatively constant versus dilute layer concentration, despite a ~50% reduction in the number SubNc molecules in the total donor layer. This trend indicates that the internal efficiency increases with dilution. The reduction in V_{OC} upon dilution is corroborated by an increase in forward-bias dark current upon dilution. Of additional interest, the fill factor increases with dilution in the control device to 75 wt % SubNc and remains constant upon further dilution. A similar trend has been reported previously for dilutions of C_{60} in UGH2.[43] This may suggest a shift in the steady state charge density upon

DOI: 10.1021/am508332n
ACS Appl. Mater. Interfaces 2015, 7, 2912−2918

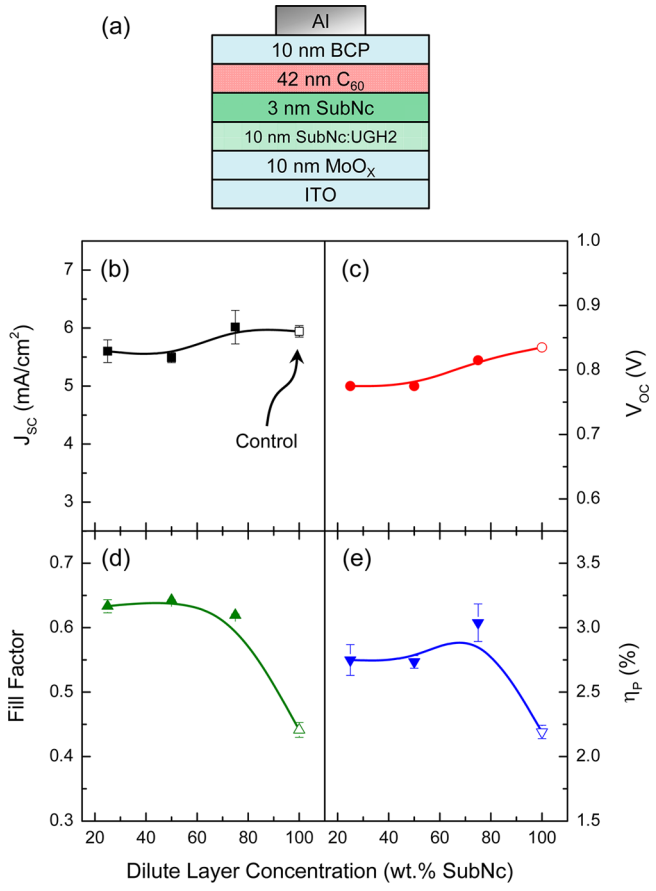

Figure 3. (a) Schematic of a host–guest device based on the pairing of SubNc and UGH2. (b–e) Short-circuit current density (J_{SC}), open-circuit voltage (V_{OC}), fill factor, and power conversion efficiency (η_P) at an intensity of 100 mW/cm^2 under AM1.5G simulated solar illumination for the host–guest device as a function of dilute layer concentration. The open symbols refer to a device with a donor layer consisting of a single 13 nm-thick layer of SubNc.

dilution at voltages below V_{OC}, thereby reducing either nongeminate recombination at the donor–acceptor interface or exciton-polaron annihilation near the extraction layers.[44,45] Overall, the η_P is optimized at η_P = (3.0 ± 0.1)% for a dilute layer concentration of 75 wt % SubNc. As in the case of host–guest donor layers consisting of SubPc and UGH2, the optimum η_P is achieved when the donor layer is partially diluted.

2.3. Dilute SubNc Devices with a Photoactive Host. In order to recover the lost absorption that occurs in host–guest donor layers containing UGH2, devices employing a photoactive host of SubPc were examined. Recall from Figure 1 that the molecular orbital energy levels for SubNc are favorably nested within those of SubPc, similar to the host–guest relationship between UGH2 and SubNc. The device architecture is shown in Figure 4, with the dilute layer consisting of a 10 nm-thick layer of 25 wt % SubNc in SubPc. As can be seen from the current density–voltage characteristics in Figure 4b, the use of a photoactive host increases the J_{SC} from (5.6 ± 0.2) to (6.2 ± 0.1) mA/cm^2 over devices using an UGH2 host. Interestingly, the V_{OC} increases from (0.78 ± 0.01) to (0.85 ± 0.01) V upon replacing UGH2 with SubPc, similar to the value measured for the undiluted control device and consistent with the measured reduction in forward bias dark current. In contrast, the fill factor for devices containing a SubPc host is larger than that measured for the control device with a value of (0.62 ± 0.01), similar to that of the device incorporating UGH2 as the host material. Incorporating SubPc as the photoactive host retains the best characteristics of the control and host–guest OPVs containing UGH2 while also leading to enhanced J_{SC} compared to both devices. The η_P is also enhanced at a value of η_P = (3.2 ± 0.1)%. Table 1 summarizes the measured device characteristics. The J_{SC} and η_P can be further enhanced by utilizing a 40 nm-thick layer of C_{70} as the acceptor layer. This strategy is common in the OPV literature as C_{70} has broader absorption than C_{60}.[46−48] With C_{70}, the J_{SC} increases to (8.7 ± 0.5) mA/cm^2 and the η_P increases to (4.3 ± 0.2)%. These represent significant enhancements relative to a SubNc/C_{70} planar heterojunction control device that shows J_{SC} = (6.0 ± 0.1) mA/cm^2, V_{OC} = (0.83 ± 0.01) V, fill factor = (0.43 ± 0.01), and η_P = (2.2 ±

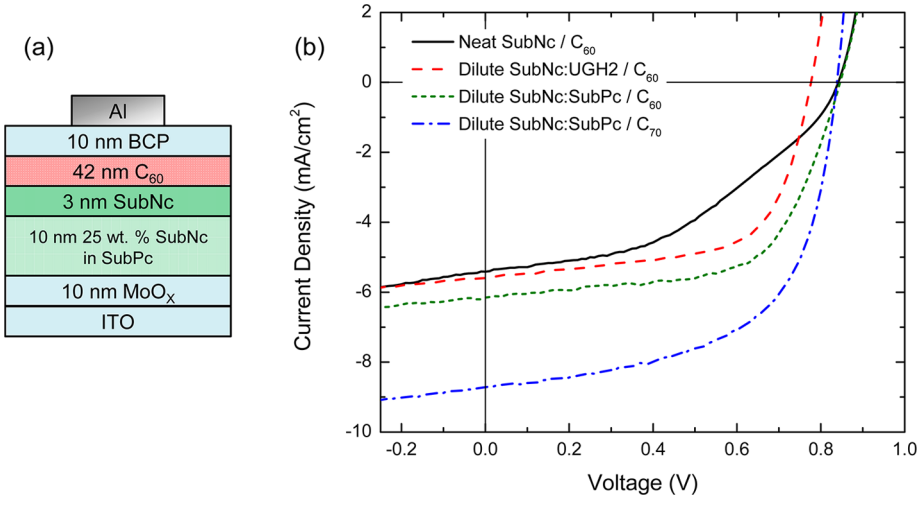

Figure 4. (a) Schematic of a host–guest OPV incorporating SubPc as a photoactive host. (b) Current density–voltage measurements at an intensity of 100 mW/cm^2 under AM1.5G solar simulated illumination for devices incorporating a neat SubNc donor layer (neat SubNc/C_{60}), a host–guest donor layer with UGH2 as the host (dilute SubNc:UGH2/C_{60}), and a host–guest donor layer with SubPc as the host (dilute SubNc:SubPc/C_{60}). Also shown is a host–guest OPV with SubPc as the host and a C_{70} acceptor layer (dilute SubNc:SubPc/C_{70}).

DOI: 10.1021/am508332n
ACS Appl. Mater. Interfaces 2015, 7, 2912−2918

Table 1. Summary of Extracted Photovoltaic Parameters from Figure 4b at an Intensity of 100 mW/cm^2 under AM 1.5G Solar Simulated Illumination

host	acceptor	J_{SC} [mA/cm^2]	V_{OC} [V]	fill factor	η_P [%]
none	C_{60}	5.4 ± 0.1	0.85 ± 0.01	0.43 ± 0.01	2.0 ± 0.1
none	C_{70}	6.0 ± 0.1	0.83 ± 0.01	0.43 ± 0.01	2.2 ± 0.1
UGH2	C_{60}	5.6 ± 0.2	0.78 ± 0.01	0.63 ± 0.01	2.8 ± 0.1
SubPc	C_{60}	6.2 ± 0.1	0.85 ± 0.01	0.62 ± 0.01	3.2 ± 0.1
SubPc	C_{70}	8.7 ± 0.5	0.84 ± 0.01	0.60 ± 0.01	4.3 ± 0.2

0.1)% under AM1.5G solar simulated illumination at an intensity of 100 mW/cm^2.

In order to examine changes in the internal quantum efficiency (η_{IQE}) of the host−guest OPVs presented hereto, the η_{EQE} and reflectivity (R) are separately measured. For this work, R is measured at an incident angle of 15° and $1 - R$ is taken as an approximate measurement of the optical absorption within the OPV. The relative η_{IQE} is calculated by dividing the η_{EQE} by $1 - R$. Transfer matrix simulations of the internal optical field permit the estimation of absorption losses within the cathode, anode, and surrounding buffer layers which can be further subtracted from $1 - R$ to provide a more accurate estimation for the absorption in the photoactive layers. Figure 5 shows the η_{EQE}, $1 - R$, and relative η_{IQE} spectra for the SubNc control device consisting of a 13 nm-thick total donor layer and a host−guest OPV consisting of a 10 nm-thick layer of 25 wt % SubNc diluted in SubPc and a 3 nm-thick neat layer of SubNc. Recall, both devices contain a 42 nm-thick film of C_{60} as the acceptor. Inspection of the η_{EQE} reveals enhancements in both the C_{60} and SubPc regions of the spectrum. The latter is clearly rationalized since the control device does not contain any SubPc. The former is likely due to an increase in the η_{CC} for the device. Since the C_{60} acceptor layer thickness and donor−acceptor interface remain constant between the control and dilute devices, changes in the acceptor exciton diffusion (η_D) and exciton dissociation efficiencies are likely minimal. Consequently, η_{CC} is the only remaining component of the η_{IQE} likely to be affected. Inspection of the dependence of fill factor on concentration for the SubNc:UGH2 host−guest OPVs further suggests that η_{CC} is not constant. Figure 5b shows $1 - R$ for these two devices and confirms that the response from SubNc is indeed reduced upon the addition of SubPc, as marked by a decrease in $1 - R$ at a wavelength (λ) = 690 nm (SubNc) and an increase in $1 - R$ at λ = 590 nm (SubPc). The relative η_{IQE} values are shown in Figure 5c, with broadband enhancement observed for the host−guest OPV with a photoactive host relative to the control device. From the earlier discussion of η_{CC}, the broadband enhancement in the relative η_{IQE} seems to be mainly a result of an enhanced η_{CC}. This is in contrast to the result obtained with SubPc:UGH2 host−guest OPVs reported previously which show large enhancements in the relative η_{IQE} upon dilution due to increases in the η_D. Though the peak relative η_{IQE} >70% is similar to the peak relative η_{IQE} reported for SubPc:UGH2, this result may indicate that there is no significant enhancement in L_D for SubNc when diluted in SubPc.

Such a contrast in the dependence of L_D on concentration between hosts suggests that the choice of the host material is critical. Moreover, the host material may serve a broader role in energy transfer than simply varying the average intermolecular separation. Here, SubPc is a less advantageous host material when comparing its impact on the L_D of SubNc relative to UGH2. Inspection of the parameters that control exciton

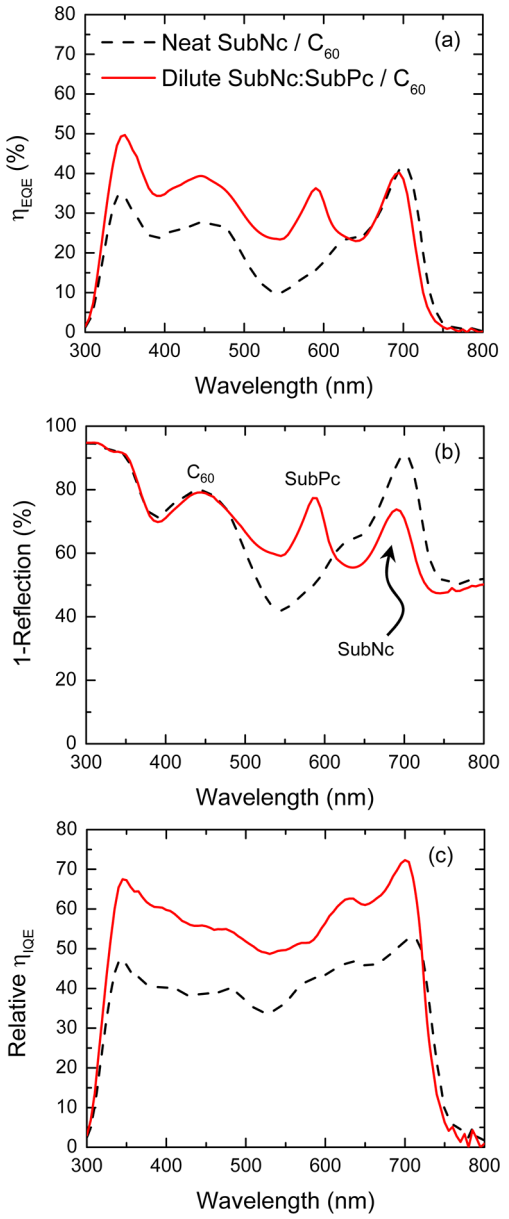

Figure 5. External quantum efficiency (a), 1 − Reflection (b), and relative internal quantum efficiency (c) spectra for a device incorporating a 13 nm-thick neat SubNc donor layer (neat SubNc/C_{60}) and a host−guest donor layer consisting of a 10 nm-thick, 25 wt % SubNc in SubPc dilute layer with a 3 nm-thick neat layer of SubNc at the interface (dilute SubNc:SubPc/C_{60}).

diffusion via Förster energy transfer lends intuition (eq 1). For example, SubPc has $n \sim 2.3$ in the region of SubNc spectral overlap whereas UGH2 has $n \sim 1.6$. The larger n serves to reduce the rate of energy transfer and therefore L_D. Additionally, the more polar nature of SubPc as compared to

DOI: 10.1021/am508332n
ACS Appl. Mater. Interfaces 2015, 7, 2912−2918

UGH2 may redshift the photoluminescence of SubNc upon dilution owing to a solid-state solvation effect.[49,50] This effect would reduce the spectral overlap integral and also reduce the L_D of SubNc when diluted in SubPc as compared to UGH2. Differences in thin-film morphology may also reduce the L_D if SubNc molecules diluted in a SubPc matrix adopt a conformation with a reduced κ. The good agreement for dilute SubNc:UGH2 experimental and predicted L_D under the assumption of randomly oriented, rigid dipoles does not suggest the presence of crystallinity for these films.

Beyond exciton transport, the host species may also affect charge transport. For a donor layer, the interplay of host and guest highest occupied molecular orbital energy levels (HOMO) will dictate the most efficient charge carrier pathway. The mixing ratio provides a route toward optimizing this interplay for a given pair of materials.

3. CONCLUSIONS

In conclusion, we have demonstrated an efficient host−guest donor layer for OPVs using an energy-cascade architecture. Efficient exciton harvesting is demonstrated from two donor materials with complementary absorption. A 10% enhancement in J_{SC} is found for host−guest OPVs with a SubPc photoactive host as compared devices with the nonabsorbing UGH2 host. Further, device measurements of the internal efficiency reveal that the 40% enhancement in η_P for host−guest devices using a C_{60} acceptor is attributable to enhancements in the η_{CC}. While the L_D for SubNc increases upon dilution in UGH2, the increase in L_D when diluted in SubPc is likely suppressed, leading to marginal increases in the η_D for this host−guest pairing, in contrast to previous work with SubPc diluted into UGH2. This relationship suggests that the selection of host material is critical, and additional properties beyond the energy-gap must be considered. Looking forward, the host−guest framework for energy-cascade OPVs shows great promise for achieving broad spectral coverage with little added complexity to current state-of-the-art planar heterojunction OPVs.

4. EXPERIMENTAL SECTION

4.1. Thin Film and Device Preparation. Organic thin films for measurements of photoluminescence were grown on glass substrates. Organic photovoltaic cells were fabricated on glass slides coated with a 150 nm-thick layer of indium−tin-oxide (ITO) having a sheet resistance of 15 Ω/□. All substrates were cleaned with tergitol and solvents. Additionally, ITO substrates were exposed to a UV−ozone ambient for 10 min prior to the deposition of the active layers. Organic layers were deposited via vacuum thermal sublimation (<10^{-7} Torr) at a nominal rate of 0.2 nm/s. Devices were capped with a 100 nm-thick cathode layer of Al deposited at a nominal rate of 0.3 nm/s through a shadow mask defining an active area with a diameter of 1 mm. SubPc, SubNc, and UGH2 were purchased from Luminescence Technology Corporation, and C_{60} was purchased from MER Corporation. All materials were used as received with no further purification.

4.2. Optoelectronic Characterization. Photoluminescence quenching data were recorded using a Photon Technology International Quantum Master 4 Fluorometer. All PL measurements were performed under an N_2 purge. Photoluminescence quenching measurements were made at an incident angle of 70° to the substrate normal. The excitation source was a monochromatic xenon lamp selected to a wavelength of λ = 600 nm. All film thicknesses and optical constants were measured using a J. A. Woollam spectroscopic ellipsometer. Film thicknesses were fit using a Cauchy model. External quantum efficiency testing was performed under illumination from a 300 W xenon lamp coupled to a Cornerstone 130 1/8 m monochromator and chopped with a Stanford Research Systems SR540 optical chopper. Electrical characteristics were measured using a Stanford Research Systems SR810 lock-in amplifier. Device parameters were extracted from current−voltage testing at an intensity of (100 ± 5) mW/cm^2 under AM1.5G solar simulated illumination.

■ ASSOCIATED CONTENT

Supporting Information

SubNc exciton diffusion length, planar heterojunction devices based on neat films of SubNc, current density−voltage characteristics of dilute SubNc devices with a nonabsorbing host, current density−voltage characteristics for a planar heterojunction device with a neat SubNc donor layer and a C_{70} acceptor layer, atomic force microscopy for the quencher HATCN. This material is available free of charge via the Internet at http://pubs.acs.org.

■ AUTHOR INFORMATION

Corresponding Author

*E-mail: rholmes@umn.edu.

Notes

The authors declare no competing financial interest.

■ ACKNOWLEDGMENTS

This work was supported by the National Science Foundation (NSF) under DMR-1307066. S.M.M. also acknowledges support from a University of Minnesota Doctoral Dissertation Fellowship. The authors graciously thank Thomas R. Fielitz for performing the atomic force microscopy (AFM).

■ REFERENCES

(1) Li, G.; Zhu, R.; Yang, Y. Polymer Solar Cells. *Nat. Photonics* **2012**, *6*, 153−161.

(2) He, Z.; Zhong, C.; Su, S.; Xu, M.; Wu, H.; Cao, Y. Enhanced Power-Conversion Efficiency in Polymer Solar Cells Using an Inverted Device Structure. *Nat. Photonics* **2012**, *6*, 591−595.

(3) Cabanetos, C.; El Labban, A.; Bartelt, J. A.; Douglas, J. D.; Mateker, W. R.; Fréchet, J. M. J.; McGehee, M. D.; Beaujuge, P. M. Linear Side Chains in Benzo1,2-b:4,5-b′]Dithiophene-Thieno3,4-c]Pyrrole-4,6-Dione Polymers Direct Self-Assembly and Solar Cell Performance. *J. Am. Chem. Soc.* **2013**, *135*, 4656−4659.

(4) Halls, J. J. M.; Walsh, C. A.; Greenham, N. C.; Marseglia, E. A.; Friend, R. H.; Moratti, S. C.; Holmes, A. B. Efficient Photodiodes from Interpenetrating Polymer Networks. *Nature* **1995**, *376*, 498−500.

(5) Yu, G.; Gao, J.; Hummelen, J. C.; Wudl, F.; Heeger, A. J. Polymer Photovoltaic Cells: Enhanced Efficiencies via a Network of Internal Donor-Acceptor Heterojunctions. *Science* **1995**, *270*, 1789−1791.

(6) Zou, Y.; Holst, J.; Zhang, Y.; Holmes, R. J. 7.9% Efficient Vapor-Deposited Organic Photovoltaic Cells Based on a Simple Bulk Heterojunction. *J. Mater. Chem. A* **2014**, *2*, 12397.

(7) Cowan, S. R.; Roy, A.; Heeger, A. J. Recombination in Polymer-Fullerene Bulk Heterojunction Solar Cells. *Phys. Rev. B* **2010**, *82*, 245207.

(8) Hawks, S. A.; Deledalle, F.; Yao, J.; Rebois, D. G.; Li, G.; Nelson, J.; Yang, Y.; Kirchartz, T.; Durrant, J. R. Relating Recombination, Density of States, and Device Performance in an Efficient Polymer:-Fullerene Organic Solar Cell Blend. *Adv. Energy Mater.* **2013**, *3*, 1201−1209.

(9) Lakhwani, G.; Rao, A.; Friend, R. H. Bimolecular Recombination in Organic Photovoltaics. *Annu. Rev. Phys. Chem.* **2014**, *65*, 557−581.

(10) Heremans, P.; Cheyns, D.; Rand, B. P. Strategies for Increasing the Efficiency of Heterojunction Organic Solar Cells: Material Selection and Device Architecture. *Acc. Chem. Res.* **2009**, *42*, 1740−1747.

(11) Menke, S. M.; Holmes, R. J. Exciton Diffusion in Organic Photovoltaic Cells. *Energy Environ. Sci.* **2014**, *7*, 499−512.

DOI: 10.1021/am508332n
ACS Appl. Mater. Interfaces 2015, 7, 2912−2918

(12) Foertig, A.; Wagenpfahl, A.; Gerbich, T.; Cheyns, D.; Dyakonov, V.; Deibel, C. Nongeminate Recombination in Planar and Bulk Heterojunction Organic Solar Cells. *Adv. Energy Mater.* **2012**, *2*, 1483−1489.
(13) Menke, S. M.; Luhman, W. A.; Holmes, R. J. Tailored Exciton Diffusion in Organic Photovoltaic Cells for Enhanced Power Conversion Efficiency. *Nat. Mater.* **2013**, *12*, 152−157.
(14) Mullenbach, T. K.; McGarry, K. A.; Luhman, W. A.; Douglas, C. J.; Holmes, R. J. Connecting Molecular Structure and Exciton Diffusion Length in Rubrene Derivatives. *Adv. Mater.* **2013**, *25*, 3689−3693.
(15) Verreet, B.; Heremans, P.; Stesmans, A.; Rand, B. P. Microcrystalline Organic Thin-Film Solar Cells. *Adv. Mater.* **2013**, *25*, 5504−5507.
(16) Cnops, K.; Rand, B. P.; Cheyns, D.; Verreet, B.; Empl, M. A.; Heremans, P. 8.4% Efficient Fullerene-Free Organic Solar Cells Exploiting Long-Range Exciton Energy Transfer. *Nat. Commun.* **2014**, *5*, 3406.
(17) Barito, A.; Sykes, M. E.; Huang, B.; Bilby, D.; Frieberg, B.; Kim, J.; Green, P. F.; Shtein, M. Universal Design Principles for Cascade Heterojunction Solar Cells with High Fill Factors and Internal Quantum Efficiencies Approaching 100%. *Adv. Energy Mater.* **2014**, *4*, 1400216.
(18) Griffith, O. L.; Forrest, S. R. Exciton Management in Organic Photovoltaic Multidonor Energy Cascades. *Nano Lett.* **2014**, *14*, 2353−2358.
(19) Ichikawa, M.; Takekawa, D.; Jeon, H.; Banoukepa, G. D. Cascade-Type Excitation Energy Relay in Organic Thin-Film Solar Cells. *Org. Electron.* **2013**, *14*, 814−820.
(20) Zhou, Y.; Taima, T.; Kuwabara, T.; Takahashi, K. Efficient Small-Molecule Photovoltaic Cells Using a Crystalline Diindenoperylene Film as a Nanostructured Template. *Adv. Mater.* **2013**, *25*, 6069−6075.
(21) Schlenker, C. W.; Barlier, V. S.; Chin, S. W.; Whited, M. T.; McAnally, R. E.; Forrest, S. R.; Thompson, M. E. Cascade Organic Solar Cells. *Chem. Mater.* **2011**, *23*, 4132−4140.
(22) Luhman, W. A.; Holmes, R. J. Enhanced Exciton Diffusion in an Organic Photovoltaic Cell by Energy Transfer Using a Phosphorescent Sensitizer. *Appl. Phys. Lett.* **2009**, *94*, 153304.
(23) Rand, B. P.; Schols, S.; Cheyns, D.; Gommans, H.; Girotto, C.; Genoe, J.; Heremans, P.; Poortmans, J. Organic Solar Cells with Sensitized Phosphorescent Absorbing Layers. *Org. Electron.* **2009**, *10*, 1015−1019.
(24) Lin, C.; Nichols, V. M.; Cheng, Y.; Bardeen, C. J.; Wei, M.; Liu, S.; Lee, C.; Su, W.; Chiu, T.; Han, H.; Chen, L.; Chen, C.; Lee, J. Chloroboron Subphthalocyanine/C60 Planar Heterojunction Organic Solar Cell with *N,N*-Dicarbazolyl-3,5-Benzene Blocking Layer. *Sol. Energy Mater. Sol. Cells* **2014**, *122*, 264−270.
(25) Holmes, R. J.; D'Andrade, B. W.; Forrest, S. R.; Ren, X.; Li, J.; Thompson, M. E. Efficient, Deep-Blue Organic Electrophosphorescence by Guest Charge Trapping. *Appl. Phys. Lett.* **2003**, *83*, 3818−3820.
(26) Cnops, K.; Rand, B. P.; Cheyns, D.; Heremans, P. Enhanced Photocurrent and Open-Circuit Voltage in a 3-Layer Cascade Organic Solar Cell. *Appl. Phys. Lett.* **2012**, *101*, 143301.
(27) Barito, A.; Sykes, M. E.; Bilby, D.; Amonoo, J.; Jin, Y.; Morris, S. E.; Green, P. F.; Kim, J.; Shtein, M. Recovering Lost Excitons in Organic Photovoltaics Using a Transparent Dissociation Layer. *J. Appl. Phys.* **2013**, *113*, 203110.
(28) Chen, M. C.; Liaw, D. J.; Huang, Y. C.; Wu, H. Y.; Tai, Y. Improving the Efficiency of Organic Solar Cell with a Novel Ambipolar Polymer to Form Ternary Cascade Structure. *Sol. Energy Mater. Sol. Cells* **2011**, *95*, 2621−2627.
(29) Ameri, T.; Khoram, P.; Min, J.; Brabec, C. J. Organic Ternary Solar Cells: A Review. *Adv. Mater.* **2013**, *25*, 4245−4266.
(30) Wang, J.; Shi, S.; Leung, C.; Lau, S.; Wong, K.; Chan, P. K. Short Circuit Current Improvement in Planar Heterojunction Organic Solar Cells by Multijunction Charge Transfer. *Appl. Phys. Lett.* **2012**, *100*, 053301.
(31) Ma, B.; Woo, C. H.; Miyamoto, Y.; Fréchet, J. M. J. Solution Processing of a Small Molecule, Subnaphthalocyanine, for Efficient Organic Photovoltaic Cells. *Chem. Mater.* **2009**, *21*, 1413−1417.
(32) Cheyns, D.; Rand, B. P.; Heremans, P. Organic Tandem Solar Cells with Complementary Absorbing Layers and a High Open-Circuit Voltage. *Appl. Phys. Lett.* **2010**, *97*, 033301.
(33) Lunt, R. R.; Giebink, N. C.; Belak, A. A.; Benziger, J. B.; Forrest, S. R. Exciton Diffusion Lengths of Organic Semiconductor Thin Films Measured by Spectrally Resolved Photoluminescence Quenching. *J. Appl. Phys.* **2009**, *105*, 053711.
(34) Bergemann, K. J.; Forrest, S. R. Measurement of Exciton Diffusion Lengths in Optically Thin Organic Films. *Appl. Phys. Lett.* **2011**, *99*, 243303.
(35) Liao, L. S.; Klubek, K. P. Power Efficiency Improvement in a Tandem Organic Light-Emitting Diode. *Appl. Phys. Lett.* **2008**, *92*, 223311.
(36) Pettersson, L. A. A.; Roman, L. S.; Inganas, O. Modeling Photocurrent Action Spectra of Photovoltaic Devices Based on Organic Thin Films. *J. Appl. Phys.* **1999**, *86*, 487−496.
(37) Luhman, W. A.; Holmes, R. J. Investigation of Energy Transfer in Organic Photovoltaic Cells and Impact on Exciton Diffusion Length Measurements. *Adv. Funct. Mater.* **2011**, *21*, 764−771.
(38) Fennel, F.; Lochbrunner, S. Long Distance Energy Transfer in a Polymer Matrix Doped with a Perylene Dye. *Phys. Chem. Chem. Phys.* **2011**, *13*, 3527−3533.
(39) Förster, T. 10th Spiers Memorial Lecture. Transfer Mechanisms of Electronic Excitation. *Discuss. Faraday Soc.* **1959**, *27*, 7.
(40) Maksimov, M. Z.; Rozman, I. M. On Energy Transfer in Solid Solutions. *Opt. Spectrosc.* **1962**, *12*, 337.
(41) Zou, Y.; Holmes, R. J. Influence of a MoOx Interlayer on the Open-Circuit Voltage in Organic Photovoltaic Cells. *Appl. Phys. Lett.* **2013**, *103*, 053302.
(42) Gommans, H.; Verreet, B.; Rand, B. P.; Muller, R.; Poortmans, J.; Heremans, P.; Genoe, J. On the Role of Bathocuproine in Organic Photovoltaic Cells. *Adv. Funct. Mater.* **2008**, *18*, 3686−3691.
(43) Menke, S. M.; Lindsay, C. D.; Holmes, R. J. Optical Spacing Effect in Organic Photovoltaic Cells Incorporating a Dilute Acceptor Layer. *Appl. Phys. Lett.* **2014**, *104*, 243302.
(44) Verreet, B.; Bhoolokam, A.; Brigeman, A.; Dhanker, R.; Cheyns, D.; Heremans, P.; Stesmans, A.; Giebink, N. C.; Rand, B. P. Reducing Exciton-Polaron Annihilation in Organic Planar Heterojunction Solar Cells. *Phys. Rev. B* **2014**, *90*, 115304.
(45) Bartynski, A. N.; Trinh, C.; Panda, A.; Lassiter, B. E.; Bergemann, K.; Zimmerman, J. D.; Forrest, S. R.; Thompson, M. E. A Fullerene-Based Organic Exciton Blocking Layer with High Electron Conductivity. *Nano Lett.* **2013**, *13*, 3315−3320.
(46) Wang, X.; Perzon, E.; Oswald, F.; Langa, F.; Admassie, S.; Andersson, M. R.; Inganäs, O. Enhanced Photocurrent Spectral Response in Low-Bandgap Polyfluorene and C70-Derivative-Based Solar Cells. *Adv. Funct. Mater.* **2005**, *15*, 1665−1670.
(47) Pfuetzner, S.; Meiss, J.; Petrich, A.; Riede, M.; Leo, K. Improved Bulk Heterojunction Organic Solar Cells Employing C70 Fullerenes. *Appl. Phys. Lett.* **2009**, *94*, 223307.
(48) Pandey, R.; Zou, Y.; Holmes, R. J. Efficient, Bulk Heterojunction Organic Photovoltaic Cells Based on Boron Subphthalocyanine Chloride-C-70. *Appl. Phys. Lett.* **2012**, *101*, 033308.
(49) Bulović, V.; Deshpande, R.; Thompson, M. E.; Forrest, S. R. Tuning the Color Emission of Thin Film Molecular Organic Light Emitting Devices by the Solid State Solvation Effect. *Chem. Phys. Lett.* **1999**, *308*, 317−322.
(50) Baldo, M. A.; Soos, Z. G.; Forrest, S. R. Local Order in Amorphous Organic Molecular Thin Films. *Chem. Phys. Lett.* **2001**, *347*, 297−303.

DOI: 10.1021/am508332n
ACS Appl. Mater. Interfaces 2015, 7, 2912−2918